Global Energy Interconnection
Development and Cooperation Organization

ELSEVIER
Production And Hosting By Elsevier On Behalf Of KeAi
KeAi

Volume 7 Number 6 December 2024 (786-797)
DOI: 10.1016/j.gloei.2024.11.004

Global Energy Interconnection

Contents lists available at ScienceDirect
https: //www.sciencedirect.com/journal/global-energy-interconnection

Full-length article

Flexible linear clock–based distributed self-triggered active power-sharing secondary control of AC microgrids

Yulin Chen[1,2,3], Xing Huang[3], Guangxin Zhi[2], Shaohua Yang[4], Hongxun Hui[4], Donglian Qi[2,3], Yunfeng Yan[3], Fengkai Gao[1]

1. Key Laboratory of Modern Power System Simulation and Control & Renewable Energy Technology, Ministry of Education (Northeast Electric Power University), Jilin, 132012, P. R. China
2. Hainan Institute, Zhejiang University, Sanya, 572000, P. R. China
3. College of Electrical Engineering, Zhejiang University, Hangzhou, 310027, P. R. China
4. State Key Laboratory of Internet of Things for Smart City, University of Macau, Macao, 999078, P. R. China

Scan for more details

Abstract: Traditional active power sharing in microgrids, achieved by the distributed average consensus, requires each controller to continuously trigger and communicate with each other, which is a wasteful use of the limited computation and communication resources of the secondary controller. To enhance the efficiency of secondary control, we developed a novel distributed self-triggered active power-sharing control strategy by introducing the signum function and a flexible linear clock. Unlike continuous communication–based controllers, the proposed self-triggered distributed controller prompts distributed generators to perform control actions and share information with their neighbors only at specific time instants monitored by the linear clock. Therefore, this approach results in a significant reduction in both the computation and communication requirements. Moreover, this design naturally avoids Zeno behavior. Furthermore, a modified triggering condition was established to achieve further reductions in computation and communication. The simulation results confirmed that the proposed control scheme achieves distributed active power sharing with very few controller triggers, thereby substantially enhancing the efficacy of secondary control in MGs.

Keywords: Active power sharing; Distributed secondary control; Self-triggered mechanism; AC microgrid; Control efficiency

Received: 11 April 2024/Revised: 28 May 2024/Accepted: 11 June 2024/
Published: 25 December 2024

✉ Guangxin Zhi
zhiguangxin@zju.edu.cn

Yulin Chen
chenyl2017@zju.edu.cn

Xing Huang
xinghuang@zju.edu.cn

Shaohua Yang
shaohuayang2022@gmail.com

Hongxun Hui
hongxunhui@um.edu.mo

Donglian Qi
qidl@zju.edu.cn

Yunfeng Yan
21210004@zju.edu.cn

Fengkai Gao
fk.gao@neepu.edu.cn

0 Introduction

To jointly cope with the critical challenges posed by climate change, the Chinese Government promised that it will strive to achieve peak carbon emissions by 2030 and carbon neutrality by 2060. Consequently, China decided to construct a new power system using renewable energy (RE) as the main source of power generation. Therefore, RE sources (e.g., photovoltaic and wind power) are being rapidly developed and integrated into new power systems

to combat climate change [1, 2]. However, uncertainties caused by the high penetration of RE would disturb the stable operation of power systems. Therefore, in the future, a new power system — distributed RE — must be utilized for system regulation.

To promote the effective utilization of RE, microgrids (MGs) are considered a promising solution for coordinating multiple distributed generators (DGs), such as photovoltaic units and wind turbines, within an area [3, 4]. The operational flexibility of MGs is crucial for enhancing the power supply reliability of RE, which can help reduce carbon emissions. MGs can be connected to the main power grid for operation or can operate independently from the grid. Diverse advanced control strategies have been explored to enhance MG flexibility. Among them, the hierarchical control structure stands out as the most widely adopted approach for constructing control systems [5-7] and is composed of primary, secondary, and tertiary control layers.

Among the three control layers, secondary control is of great importance for RE-based DGs to participate in the system regulation of islanded MGs. Thus, the present study focused on the secondary control of MGs. Typically, a centralized control structure is employed as secondary control in MGs [8]. However, centralized communication involves complicated networks and is plagued by a single point of failure. The centralized communication mode also exhibits poor scalability, making it unsuitable for MGs with numerous DGs. In response to these limitations, recent advancements have resulted in the integration of multi-agent system-based control strategies in the secondary control of MGs to enhance reliability and scalability [9]. Consequently, distributed secondary control has emerged as a preferred control scheme [10]. Numerous distributed secondary controls for MGs have been reported in the literature [11-14]. However, the majority rely on continuous time–based control and communication assumptions, which can result in the inefficient utilization of the limited communication and computing resources of local controllers [15]. Therefore, traditional distributed secondary control is unsuitable for scenarios in which a new power system will accommodate large-scale RE-based DGs in the near future.

To enhance efficiency, the implementation of distributed secondary control can minimize control actions and communication requirements by activating control processes only when necessary. This can be accomplished by using event-triggered mechanisms [16]. Consequently, numerous researchers have focused on developing distributed event-triggered controllers to address frequency restoration or power-sharing challenges with reduced communication requirements.

For instance, in [17], a sampling and holding scheme was introduced to realize reactive power-sharing control in MGs to minimize communication requirements. In [18], a distributed event-triggered control approach was developed for frequency restoration supported by distributed estimation. Furthermore, in [19], a distributed event-triggered scheme was proposed to facilitate active power-sharing control. Subsequently, through the decoupling of frequency restoration control, both active power sharing and frequency restoration control are realized using reduced communication requirements. To enhance convergence performance, in [20], the authors presented proportional-integral (PI) distributed event-triggered secondary control. Subsequently, in [21], the authors explored a finite-time distributed event-triggered secondary frequency and voltage control for islanded AC microgrids, aiming for system convergence within a specified time frame. Considering the nonlinear dynamics and unknown external disturbances, the authors of [22] constructed a hybrid event-triggered mechanism for the secondary control of frequency and voltage in islanded MGs according to the controller proposed in [23], which can reduce the triggers of controllers while alleviating external disturbances. To address denial-of-service attacks, in [24], the authors presented an event-triggered secondary control based on model-free prediction control. Nonetheless, most of the proposed controllers activated by events require constant monitoring of the triggering conditions, leading to a subsequent escalation in the computational burden. To overcome this deficiency, in [25], the authors attempted to extend the checking intervals to reduce the computation burden, and the upper boundary of the triggering condition checking period was derived to prescribe the checking intervals. However, this approach is ineffective when the triggering function is relatively complex. A more effective way to reduce computational requirements is to design a self-triggered mechanism that can predict the next event time instant using information from the preceding event [26]. For MGs, the earliest research on distributed self-triggered secondary control focused on active power-sharing control, as outlined in [27], utilizing the mechanism presented in [28]. Subsequently, the solutions for both frequency restoration and active power-sharing control were solved by the authors of [29] through the development of a novel distributed self-triggered mechanism. For the self-triggered mechanism, the usual method is to calculate the next event time according to the local and neighboring information and the reference event-triggered condition. Currently, the simplest calculation for the next event time is to solve a

quadratic function at each time instant, which would also cause a computational efficiency problem for a controller with a number of neighbors. Specifically, although the self-triggered secondary controller mentioned above can reduce the computational frequency, it increases the computational complexity at each triggering time instant. This leads to an additional computational burden. To this end, eliminating the computation process at each triggering time instant of the self-triggered secondary control for better computation and communication efficiency motivated this research.

In this study, to alleviate both the communication and computational burdens on the secondary control system, a distributed self-triggered active power-sharing control strategy was proposed. The main contributions of this study are as follows:

1) A flexible distributed self-triggered mechanism was designed by introducing a signum function to prescribe the control speed and designing a linear clock to determine event times, which eliminates the process of triggering condition computing, enabling a fully distributed active power-sharing control without computation and very few communication requirements. Moreover, the inherent exclusion of the Zeno behavior can be achieved through this mechanism.

2) A changeable clock rate was introduced to enhance the robustness and flexibility of the distributed self-triggered control. Therefore, the number of triggers can be tuned by adjusting the clock rate. The implementation of the flexible linear clock not only reduces the communication frequency but also significantly alleviates the computation requirements.

3) A modified triggering condition was developed to overcome the limitations of the proposed self-triggered controller, which would generate periodic triggers even during the steady state. With the incorporation of the modified triggering condition, the occurrence of triggers during steady states can be completely avoided, leading to a significant reduction in both communication and computation.

1 Model and control in MGs

1.1 Primary control of inverter-based DGs

In an MG with N RE-based DGs (such as photovoltaic units), the dynamics of each DG can be modeled as an inverter-based DG [26]. In each DG unit, a DC resource, DC/AC inverter, and LC filter form the hardware foundation. To make the DG generate the desired power output, the DG software is typically equipped with a cascading configuration involving inner current, inner voltage, and PWM controls. A detailed diagram of the control loops in a DG unit is shown in Fig. 1.

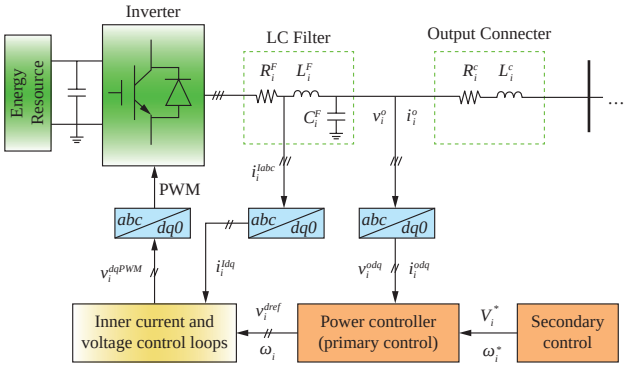

Fig. 1 Diagram of the detailed control loops in a DG

It is important to note that the inner control loops of a DG operate over very short timescales. Consequently, they can be neglected when considering secondary control levels. Therefore, for brevity, we omitted the detailed dynamics of the inner control loop. More details on these control loops can be found in [28].

The primary control of a DG must provide references for the inner current and voltage control loops, which commonly employ a droop mechanism and emulate the behavior of traditional synchronous generators. The detailed relationships of the droop mechanism can be found in [29-35]. of note, this primary control is local and does not involve communication.

As mentioned earlier, this droop mechanism–based primary control can lead to deviations in the frequency and voltage following disturbances. Therefore, secondary control is required to restore the deviations induced by this droop mechanism–based primary control, especially for an MG working in the islanded mode.

1.2 Distributed secondary control of inverter-based DGs

To address the frequency deviation caused by droop mechanism–based primary control, a secondary control is usually employed in the MG by regulating the set points of the primary control to restore the frequency to the nominal value and achieve a fair utilization profile of DGs. With a fair utilization profile, each DG contributes equally to sustaining the stable operation of the MG system, as outlined in the following equation

$$\frac{P_1}{P_1^{\max}} = \frac{P_2}{P_2^{\max}} = \cdots = \frac{P_N}{P_N^{\max}} \tag{1}$$

where $P_i^{\max}$ denotes the maximum output active power of DG i.

The control objectives of frequency restoration and active power sharing can be mathematically expressed as follows:

$$\lim_{t\to\infty}\left|\omega_i-\omega^r\right|=0 \tag{2a}$$

$$\lim_{t\to\infty}\left|\frac{P_i}{P_i^{\max}}-\frac{P_j}{P_j^{\max}}\right|=0,\quad i\neq j \tag{2b}$$

where ω^r is the reference frequency of the MG.

To overcome the drawbacks of complexity and poor scalability, distributed secondary control is favored over traditional centralized secondary control owing to its better reliability and scalability.

Therefore, in this study, we focused on accurate active power sharing in an islanded MG. To achieve accurate distributed power sharing, an average consensus algorithm was introduced in [10]. The proposed controller ensures a fair utilization profile for each DG distribution, which can be mathematically expressed as follows:

$$u_i^P=-k_P\sum_{j\in\mathcal{N}_i}a_{ij}(q_i-q_j) \tag{3}$$

where $k_P>0$ is a positive control gain; $q_i=P_i/P_i^{\max}$; u_i^P is the control input; a_{ij} is the ith row and jth column element of the adjacency matrix A of the communication network among DGs; $a_{ij}=1$ means that DG i and DG j can communicate with each other, and $a_{ij}=0$ otherwise; and $\mathcal{N}_i=\{j\mid a_{ij}=1\}$ is a set of DG i's neighboring DGs.

Because the primary task of an islanded MG is to ensure as much supply and demand balance as possible, it is crucial to uphold the value of the nominal frequency, for example 50 Hz. Therefore, in this study, we assumed that the DGs units are aware of the nominal frequency value when the MG operates in the islanded mode. Consequently, a straightforward PI control was used to synchronize the system frequency. Specifically, the frequency control input was designed as follows:

$$u_i^{\omega}=\alpha^P(\omega^r-\omega_i)+\alpha^I\int(\omega^r-\omega_i)\mathrm{d}t \tag{4}$$

where α^P and α^I are the proportional and differential coefficients, respectively.

Next, both secondary objectives can be realized by regulating the set point of the droop curve by [6]

$$\omega_i=\omega_i^*+u_i^{\omega}+u_i^P-m_iP_i \tag{5}$$

From (3), we know that each controller must continuously compute the control input and communicate with its neighbors at each sampling time instant. This may result in time delays or information congestion when regulating large-scale RE-based DGs. To address this issue, in Section 2, we introduced a flexible, distributed, and self-triggered secondary control for active power sharing in MGs.

2 Flexible distributed self-triggered active power-sharing control

To effectively regulate active power sharing, a self-triggered mechanism was elaborately designed by incorporating a signum function and a linear clock, with is explained in detail below.

2.1 Clock-based self-triggered mechanism design

First, for the brevity, the consensus error can be defined as follows:

$$\mathrm{ce}_i(t)=\sum_{j\in\mathcal{N}_i}a_{ij}(q_i(t)-q_j(t)) \tag{6}$$

Next, using the signum function, we defined a new function as follows:

$$F_\varepsilon(x)=\begin{cases}\mathrm{sign}(x), & \text{if } |x|\geqslant\varepsilon\\ 0, & \text{otherwise,}\end{cases} \tag{7}$$

where ε is positive and denotes a desired system convergence error.

To eliminate unnecessary computational and communication processes, the following distributed self-triggered control protocol was designed using (8), accompanied by a flexible linear clock dynamic $\dot{\mathcal{T}}_i(t)=-h_i$, which are expressed as follows:

$$\begin{cases}u_i^P(t)=-F_\varepsilon(\widehat{\mathrm{ce}}_i(t))\\ \dot{\mathcal{T}}_i(t)=-h_i,\end{cases} \tag{8}$$

where $h_i>0$ is the rate of the local clock at DG i, and

$$\widehat{\mathrm{ce}}_i(t)=\mathrm{ce}_i(t_k^i)\text{ for }t\in[t_k^i,t_{k+1}^i), \tag{9}$$

where t_k^i represents the k-th (k=1,2,$\cdots$) event time for DG i. This update rule means that $\widehat{\mathrm{ce}}_i(t)$ is only updated at event time t_k^i. Otherwise, it remains unchanged during $[t_k^i,t_{k+1}^i)$. Accordingly, the specific relationship between u_i^P and q_i can be expressed as follows:

$$u_i^P(t)=-\begin{cases}\mathrm{sign}\left(\sum_{j\in\mathcal{N}_i}a_{ij}(q_i(t_k^i)-q_j(t_k^i))\right), & \text{if } \left|\sum_{j\in\mathcal{N}_i}a_{ij}(q_i(t_k^i)-q_j(t_k^i))\right|\geqslant\varepsilon\\ 0, & \text{otherwise.}\end{cases} \tag{10}$$

The event time of the controller can be defined as

$$t_k^i=\inf\{t>t_{k-1}^i\mid\mathcal{T}_i(t)=0\}. \tag{11}$$

From the dynamics of $\dot{\mathcal{T}}_i(t)=-h_i$, we know that clock $\mathcal{T}_i(t)$ linearly decreases with time. The following evolution

principle of $\mathcal{T}_i(t)$ was designed to prescribe the triggers:

$$\mathcal{T}_i(t^+)=\begin{cases}\max\left\{\dfrac{\beta_i|\mathrm{ce}_i(t)|}{4|\mathcal{N}_i|},\dfrac{\beta_i\varepsilon}{4|\mathcal{N}_i|}\right\}, & \text{if } \mathcal{T}_i(t)=0\\ \mathcal{T}_i(t), & \text{otherwise.}\end{cases} \tag{12}$$

where parameter β_i indicates how conservative the controller is when planning the next triggering time instant, and $|\mathcal{N}_i|$ is the cardinality number of $\mathcal{N}_i$.

Clock $\mathcal{T}_i(t)$ monitors triggering time instants and decreases with the linear dynamics of $\dot{\mathcal{T}}_i(t)=-h_i$. When $\mathcal{T}_i(t)$ decreases to zero, the controller is triggered (which is implied by (11)). Simultaneously, at this time instant, $\mathcal{T}_i(t)$ is updated by $\max\left\{\dfrac{\beta_i|\mathrm{ce}_i(t)|}{4|\mathcal{N}_i|},\dfrac{\beta_i\varepsilon}{4|\mathcal{N}_i|}\right\}$. The underlying principle of this self-triggering mechanism is illustrated in Fig. 2.

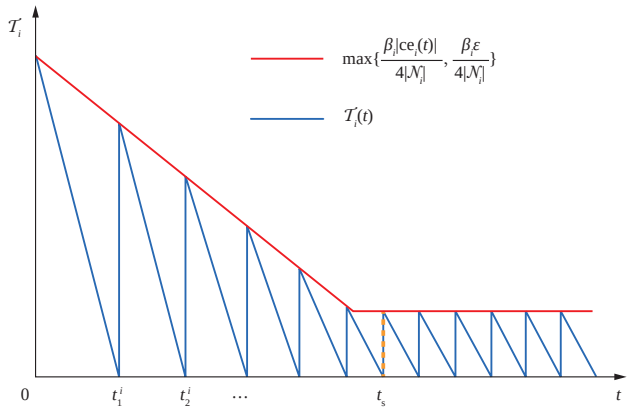

Fig. 2 Dynamic evolution of $\mathcal{T}_i(t)$

The blue line in Fig. 2 represents the evolution of $\mathcal{T}_i(t)$ and the red line represents the value of $\max\left\{\dfrac{\beta_i|\mathrm{ce}_i(t)|}{4|\mathcal{N}_i|},\dfrac{\beta_i\varepsilon}{4|\mathcal{N}_i|}\right\}$. From the evolution of $\mathcal{T}_i(t)$, the next event time of DG *i* can be defined as follows:

$$t_{k+1}^i=t_k^i+\begin{cases}\dfrac{\beta_i|\widehat{\mathrm{ce}}_i(t_k^i)|}{4h_i|\mathcal{N}_i|} & \text{if } |\mathrm{ce}_i(t_k^i)|\geqslant\varepsilon\\ \dfrac{\beta_i\varepsilon}{4h_i|\mathcal{N}_i|} & \text{if } |\mathrm{ce}_i(t_k^i)|<\varepsilon.\end{cases} \tag{13}$$

Consequently, for each DG *i*, a lower bound exists in the time interval between any two consecutive triggering instances: for any $k\geqslant 1$,

$$t_{k+1}^i-t_k^i\geqslant\frac{\beta_i\varepsilon}{4|\mathcal{N}_{\max}|}. \tag{14}$$

in which $|\mathcal{N}_{\max}|=\max\{|\mathcal{N}_i|\}$. Thus, Zeno behavior is naturally excluded in this mechanism.

It is also worth highlighting that the introduction of a linear clock eliminates the necessity for the controller to consistently compute the triggering condition function compared with existing event-triggered controls, such as the controller proposed in [18]. This implies that the proposed self-triggering mechanism can improve the efficiency of the control system in terms of both computation and communication.

Specifically, the correctness and effectiveness of the proposed distributed self-triggered mechanism are demonstrated in the following theorem:

Theorem 1: Consider *N* DGs units in an MG communicating through a connected and undirected communication topology. Each DG is regulated by the control system defined in (8) and monitored by (10) and (11). Let the parameter h_i be positive for all DG *i* values, where *i*= 1, 2, ⋯, *N*. If we let

$$\beta_i<h_i, \tag{15}$$

then the control objective of power sharing can be realized as follows:

$$\lim_{t\to\infty}\Big|\sum_{j\in\mathcal{N}_i}\Big(\frac{P_i}{P_i^{\max}}-\frac{P_j}{P_j^{\max}}\Big)\Big|\leqslant\varepsilon, \tag{16}$$

where ε is the desired convergence error.

Proof: we used the Lyapunov method to prove the stability of the proposed self-triggered controller. The candidate Lyapunov function is selected as shown below. For $t\geqslant 0$,

$$V(t)=\frac{1}{2}\boldsymbol{q}^T(t)\boldsymbol{L}\boldsymbol{q}(t)>0, \tag{17}$$

where $\boldsymbol{q}(t)=[q_1(t),q_2(t),\cdots,q_N(t)]^T$, and $\boldsymbol{L}=\mathrm{diag}\{|\mathcal{N}_i|\}-A$ is the Laplacian matrix of the communication network.

By considering the derivative of *V*(*t*), we obtain

$$\begin{aligned}\dot{V}(t)&=\boldsymbol{q}^T(t)\boldsymbol{L}\dot{\boldsymbol{q}}(t)=\boldsymbol{q}^T(t)\boldsymbol{L}\boldsymbol{u}_{\boldsymbol{q}}(t)=\boldsymbol{u}_{\boldsymbol{q}}^T(t)\boldsymbol{L}\boldsymbol{q}(t)\\&=-\sum_{i=1}^{N}\Big[\sum_{j\in\mathcal{N}_i}(q_i(t)-q_j(t))\Big]\mathrm{sign}_\varepsilon(\widehat{\mathrm{ce}}_i(t))\\&=-\sum_{i:|\widehat{\mathrm{ce}}_i(t)|\geqslant\varepsilon}\mathrm{ce}_i(t)\mathrm{sign}_\varepsilon(\widehat{\mathrm{ce}}_i(t))\end{aligned} \tag{18}$$

where $\boldsymbol{u}_{\boldsymbol{q}}(t)=[u_{q_1}(t),u_{q_2}(t),\cdots,u_{q_N}(t)]^T$. Here, we used the truth that $\boldsymbol{L}$ is symmetric.

Subsequently, from (13), we can infer that, for $t\in[t_k^i,t_{k+1}^i)$, if $\widehat{\mathrm{ce}}_i(t)\leqslant-\varepsilon$, then

$$\begin{aligned}\mathrm{ce}_i(t)&\leqslant\widehat{\mathrm{ce}}_i(t)+2|\mathcal{N}_i|(t-t_k^i)\\&\leqslant\widehat{\mathrm{ce}}_i(t)-2|\mathcal{N}_i|\frac{\beta_i|\widehat{\mathrm{ce}}_i(t)|}{2|\mathcal{N}_i|h_i}\\&\leqslant\widehat{\mathrm{ce}}_i(t)(1-\frac{\beta_i}{h_i}).\end{aligned} \tag{19}$$

Similarly, an analogous inequality holds if $\widehat{\mathrm{ce}}_i(t)\geqslant\varepsilon$; then

$$\mathrm{ce}_i(t) \geqslant \widehat{\mathrm{ce}}_i(t)\left(1-\frac{\beta_i}{h_i}\right), \tag{20}$$

Inequalities (19) and (20) imply that, if $\beta_i < h_i$, then $|\widehat{\mathrm{ce}}_i(t)| \geqslant \varepsilon$, $\mathrm{ce}_i(t)$, and $|\widehat{\mathrm{ce}}_i(t)|$ have the same positive and negative sign. Therefore, for $\beta_i < h_i$,

$$\begin{aligned}\mathrm{ce}_i(t)\mathrm{sign}_\varepsilon(\widehat{\mathrm{ce}}_i(t)) \;&= \mathrm{ce}_i(t)\mathrm{sign}(\mathrm{ce}_i(t)) = \\ &|\mathrm{ce}_i(t)| \geqslant |\widehat{\mathrm{ce}}_i(t)|\left(1-\frac{\beta_i}{h_i}\right)\end{aligned} \tag{21}$$

As a result, recalling (19), we obtain

$$\begin{aligned}\dot{V}(t) \;&\leqslant -\sum_{i:|\widehat{\mathrm{ce}}_i(t)|\geqslant\varepsilon}|\widehat{\mathrm{ce}}_i(t)|\left(1-\frac{\beta_i}{h_i}\right) \leqslant \\ &-\sum_{i:|\widehat{\mathrm{ce}}_i(t)|\geqslant\varepsilon}\varepsilon\left(1-\frac{\beta_i}{h_i}\right).\end{aligned} \tag{22}$$

Inequality (22) implies that, when the time comes to t_s such that $|\widehat{\mathrm{ce}}_i(t)| < \varepsilon$ holds for every DG i, then $\dot{V}(t) = 0$ holds for all k values with $t_k^i \geqslant t_s$. Otherwise, there would exist some triggers with $\dot{V}(t) \leqslant -\varepsilon\left(1-\frac{\beta_i}{h_i}\right)$. This results in $V(t) < 0$ because of $\beta_i < h_i$. This finding violates the assumption that $V(t)$ is positive. Therefore, we conclude the proof.

Remark 1: As indicated in (16), the convergence is not an asymptotic convergence, that is, an ε of zero exists for the errors. However, errors can be minimized by selecting a sufficiently small value for ε. In other words, if we set ε as zero, the proposed control will degrade to the conventional active power-sharing control. In addition, from (13), it is evident that the choice of ε not only influences the convergence error but also determines the frequency of controller triggering. A larger ε value results in fewer triggering instances. Thus, the trade-off between the number of triggers and the convergence error should be balanced according to the practice when implementing the proposed controller.

Remark 2: This design ensures the convergence of the controller for DG i under the condition of an arbitrarily large yet finite clock rate ($h_i > 0$) provided that β_i is sufficiently small. Theoretically, h_i can be arbitrarily large. A higher h_i value corresponds to a faster clock and more triggers for the controller. Although excessive triggering is a drawback from the point of view of control efficiency, it does not affect the convergence. Conversely, a smaller h_i value implies a slower clock with fewer triggers for the controller. However, an excessively slow clock may disrupt the proper functioning of the control system, leading to a loss of convergence.

2.2 Modification of the triggering condition

From (11), the triggering condition of the proposed distributed self-triggered controller is $\mathcal{T}_i(t) = 0$. Because the introduced clock decays continuously with $\dot{\mathcal{T}}_i(t) = -h_i$, along with the mechanism described in (11), the controller triggers at a fixed frequency when it reaches a steady state. This is also clearly illustrated in Fig. 2 when $t > t_s$. This implies that the proposed controller can reduce more triggers during transient processes than during steady state. From this perspective, continuous triggering in a steady state is wasteful. We hope that the controller will remain silent in a steady state. However, the triggering condition and mechanism in (11) prescribe this.

To reduce unnecessary triggers in a steady state, a feasible method is to change the triggering conditions. From Fig. 2, we can infer that it is only necessary to trigger the controller before t_s. The characteristic of $\mathcal{T}_i$ before t_s is expressed as $\mathcal{T}_i(t^+) > \frac{\beta_i\varepsilon}{4|\mathcal{N}_i|}$. Therefore, we modified the event times using the following new triggering conditions:

$$t_k^i = \inf\{t > t_{k-1}^i \,|\, \mathcal{T}_i(t) = 0 \;\&\; 4|\mathcal{N}_i|\,\mathcal{T}_i(t^+) > \beta_i\varepsilon\}. \tag{23}$$

Through this modification, unnecessary triggers during the steady state can be effectively avoided, as shown in Fig. 3, which is demonstrated by the simulation cases in Section 3.

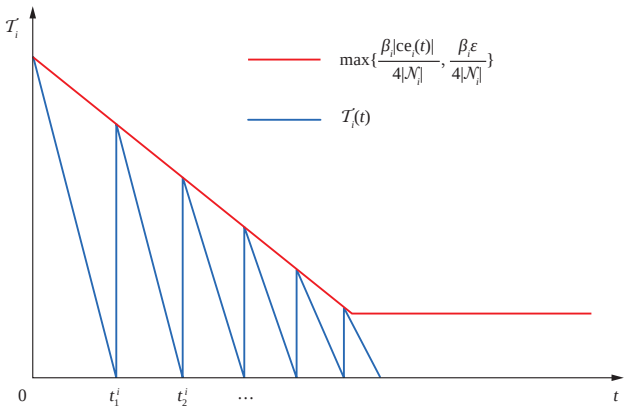

Fig. 3 The dynamic evolution of $\mathcal{T}_i(t)$ after modification

Subsequently, by incorporating the local frequency restoration control described in (4), both the objectives outlined in (2a) and (2b) of secondary control can be accomplished in a completely decentralized manner, leading to decreased requirements for both communication and computation processes.

3 Results and Verification

In this section, the results are presented to verify the efficacy of the proposed control. First, an MG model with four DGs was constructed in a MATLAB/Simulink environment. Moreover, a detailed model was built for

the DG according to the model reported in [12], which incorporates detailed inner current, inner voltage, and PWM controls. A diagram of the MG model is shown in Fig. 4, in which the blue dotted line represents the communication link and the black solid line represents the power line of the MG. In this study, we used the same parameters as those used for testing the MG in [6].

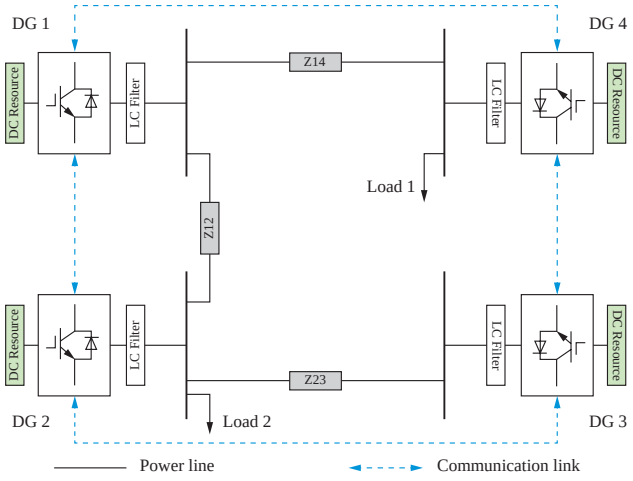

Fig. 4 Test MG with four DGs

Herein, four cases are presented to demonstrate the efficacy and superiority of the proposed distributed self-triggered active power-sharing controller. For all the cases, we set the time step to 1 ms and the desired convergence error to $t = 0$ s. The nominal frequency was set to 50 Hz.

For each case, the system saturation is as follows: at $t = 0$ s, the MG was isolated from the main grid. The secondary control then started at $t = 0.5$ s. At $t = 2$ s, load 1 decreased by 5 kW. Subsequently, load 2 increased by 5 kW at $t = 3.5$ s. For all the simulations, we showed the system performance for 5 s.

3.1 Case 1: Performance of the Self-Triggered Controller

In this case, we demonstrated the performance of the proposed control. After the simulation, the secondary control performances in terms of the frequencies and active power outputs of DGs are illustrated in Figs. 5 (a) and (b), respectively. As shown in the figures, the frequency could be quickly stabilized at 0-0.5 s owing to droop mechanism–based primary control. However, the synchronous frequency deviated from 50 Hz. After the implementation of distributed secondary control at *t*=1 s, frequency deviations were corrected to reach the desired nominal value. The generated active powers of DGs were also regulated to the same utilization profile ($P_1 : P_2 : P_3 : P_4 = 5 : 5 : 4 : 4$) after t = 1 s. It is worth noting that the convergences of the outputs were linear, as triggers were generated using a signum function and a specifically designed linear clock. As illustrated, for cases where step load changes occurred at *t*=2 s and 3.5 s, accurate active power sharing was still achieved. These results validate the efficacy of the proposed self-triggered controller.

Figure 5 (c) shows the triggering time instants for each DG. The numbers on the right-hand side represent the total number of triggers for each DG. It is evident that each DG was triggered only during transient processes. In addition, the event times were aperiodic and intermittent for each DG rather than continuous. The rate of occurrence of triggers for each DG was rather low, signifying a substantial reduction

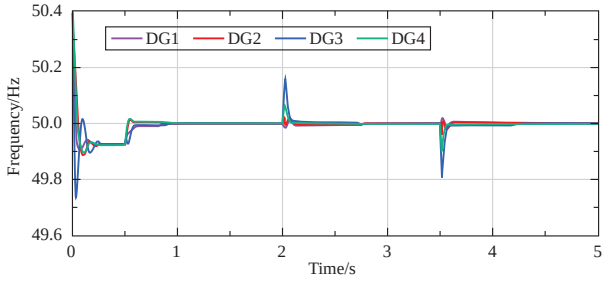

(a) Frequencies of DGs

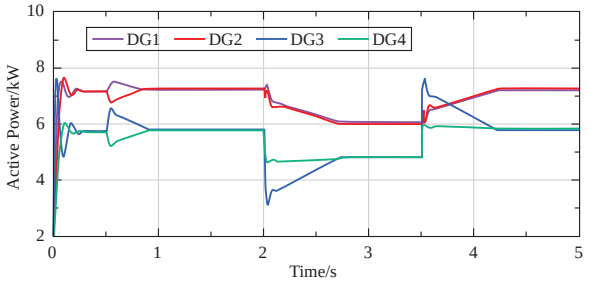

(b) Active power outputs of DGs

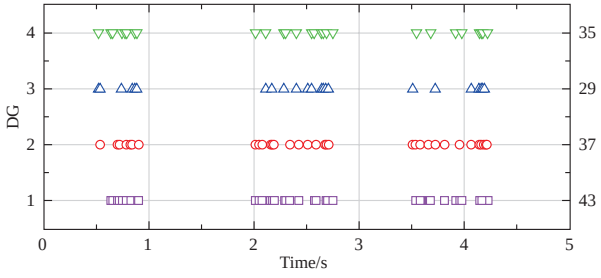

(c) Triggering time instants of DGs

Fig. 5 Performance of the proposed self-triggered control

in the communication and computational requirements for each controller.

3.2 Case 2: Necessity of the Triggering Condition Modification

In this case, we present the performance of the proposed

self-triggered control under the original triggering condition (10) to demonstrate the necessity of modifying the triggering condition. Figure 6 illustrates the active power outputs of DGs, event times of DGs, and the detailed triggers between 0.5 s and 2 s in this case. As depicted in Figs. 6 (a) and (b), the triggers during the transient processes were rare and aperiodic. However, numerous triggers were observed during the steady state, where the triggers exhibited a rare periodic pattern. This observation is consistent with the theoretical analysis described in the previous section.

A comparison between Figs. 6 (b) and 5 (c) revealed that self-triggered control, incorporating the modified triggering condition, could effectively reduce unnecessary triggers during the steady state. Consequently, the efficiency of secondary control can be remarkably improved.

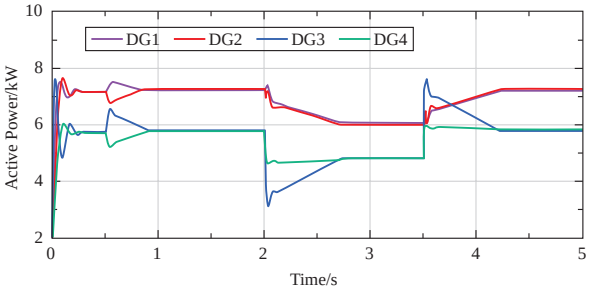

(a) Active power outputs of DGs

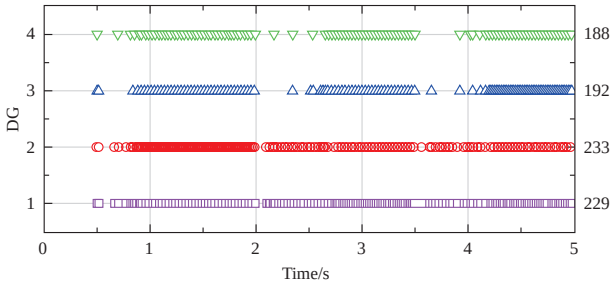

(b) Triggering time instants of DGs

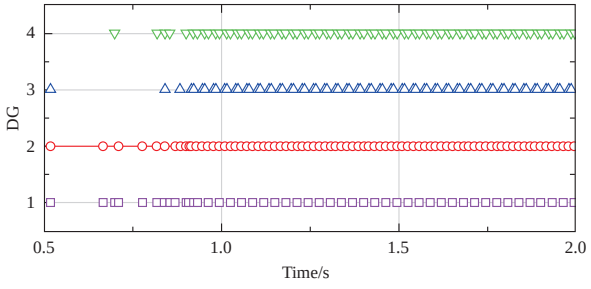

(c) Detailed triggers between 0.5 s and 2 s

Fig. 6 Performance of self-triggered control under the triggering condition (10)

3.3 Case 3: Comparison Between Traditional and Event-Triggered Controllers

To demonstrate the superiority of the proposed distributed self-triggered secondary controller, a comparative analysis was conducted against both the traditional distributed secondary controller (3) and the cutting-edge distributed event-triggered controller presented in [18]. In all scenarios, frequency restoration controls were accomplished through PI control, as outlined in (4). Therefore, only the active power-sharing control results are presented in this section.

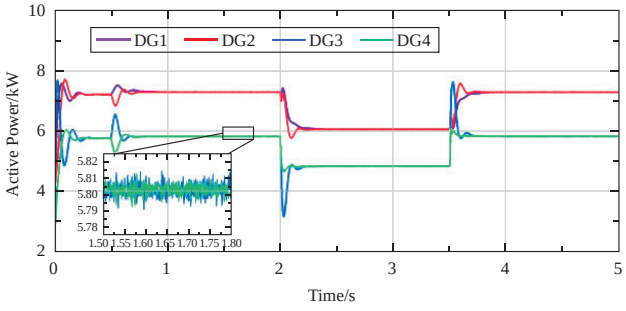

(a) The traditional controller of (3)

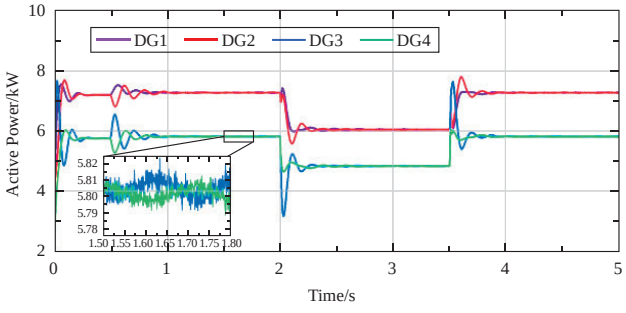

(b) The event-triggered controller in [18]

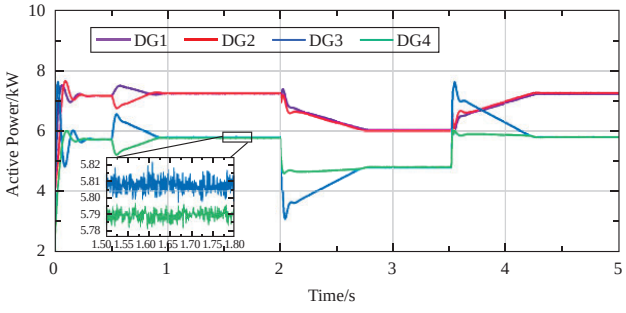

(c) The proposed self-triggered controller

Fig. 7 Output active power of each DG under

The simulation processes for all cases in this section followed the procedures outlined in Section V A. As shown in Fig.7, for both the traditional and event-triggered controllers, the sampling period for control and triggering

condition monitoring was set to 1 ms. Consequently, the traditional controller communicated 9000 times for each DG (each DG had two neighbors) in the entire simulation, whereas the event-triggered controller calculated the triggering conditions 4500 times for each DG.

Figure 8 shows the triggering time instants of each DG under three different controllers. The figure shows the distinct triggers and communication modes generated by these controllers. The traditional controller exhibited a continuous triggering and communication pattern, whereas both the even-triggered and self-triggered controllers demonstrated aperiodic and intermittent triggering and communication modes. Notably, the event-triggered controller also displayed triggers and communications during the steady state. By contrast, the proposed self-triggered controller triggered only transient processes.

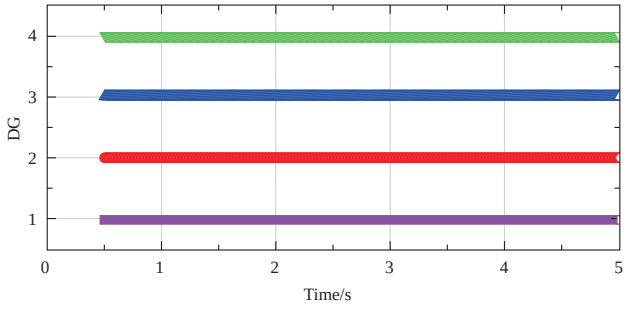

(a) The traditional controller of (3)

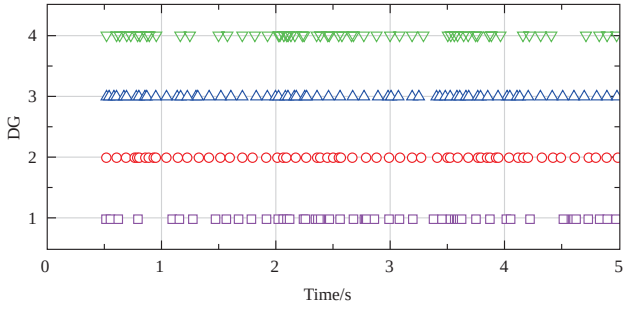

(b) The event-triggered controller in [18]

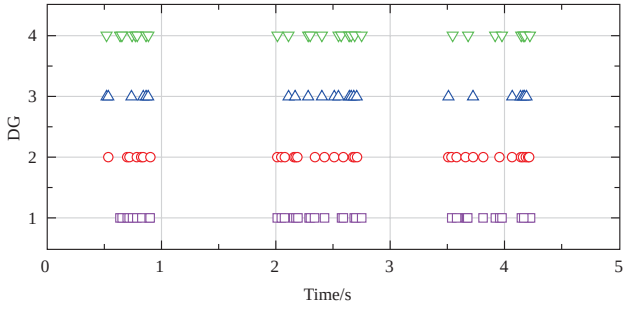

(c) The proposed self-triggered controller

Fig. 8 Triggering time instants of each DG under

Table 1 provides insights into the number of triggers (NTs), communications (NCs), and triggering condition computations (NTCCs) for each controller. Of note, the control system operated with a time step set to 1 ms. Hence, with a traditional continuous time–based controller, each DG experienced a total of NT=4500 triggering time instances. Consequently, the NC for each traditional controller was 9000 times that of the communication network. As indicated in the table, both event-triggered and self-triggered controllers resulted in a substantial reduction in the NC for each DG compared with the traditional controller, constituting approximately 4.82% and 0.8% of the NC of the traditional controller, respectively. This indicates the effectiveness of the communication reduction of event/self-triggered controllers. Notably, the self-triggered controller outperformed the event-triggered controller by reducing the number of triggers during the steady state and eliminating the need for triggering condition computations (NTCC = 0), which is a remarkable achievement in communication and computation reduction. Thus, the proposed self-triggered controller demonstrated superior performance in terms of communication and computational efficiency.

Table 1 Comparisons of NT, NC, and NTCC

Controller		DG 1	DG 2	DG 3	DG 4
Traditional Controller	NT	4500	4500	4500	4500
	NC	9000	9000	9000	9000
	NTCC	0	0	0	0
Event-triggered Controller	NT	160	154	255	301
	NC	320	308	510	602
	NTCC	4500	4500	4500	4500
Self-triggered Controller	NT	35	29	37	43
	NC	70	58	74	86
	NTCC	0	0	0	0

The results presented in this section demonstrate that the proposed self-triggered controller is superior in terms of both communication and computation cost reduction without substantially compromising the convergence performance.

3.4 Case 4: Performance at Different Clock Rates

In this section, the flexibility of the proposed control method was tested by considering different clock rates. The simulation process was identical to that described in Section V-A. Similarly, only the results are presented in this section. Without loss of generality, we let $h_i = h$ for i = 1, 2, 3, and 4.

As shown in Fig. 9 and presented in Table 2, controllers

operating at different clock rates exhibited different numbers of triggering instants. Moreover, a higher clock rate corresponded to a more frequent trigger of the controller; conversely, a lower clock rate resulted in fewer triggering time instants for the controller. Therefore, we conclude that a higher clock rate results in more efficient utilization of communication and computation resources. However, as previously analyzed, the clock rate should not be excessively small because an excessively slow clock may disrupt the proper behavior of the control system, potentially leading to a loss of convergence. Therefore, when designing a self-triggered controller, a low clock rate within acceptable conditions should be chosen.

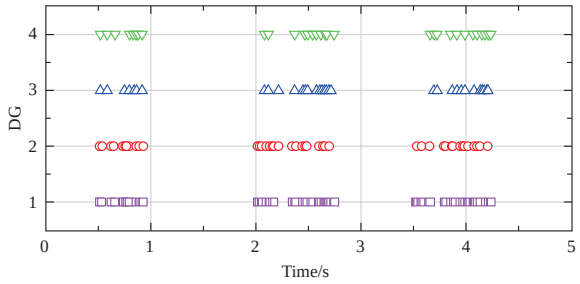

(a) $h = 2$, $\beta = 0.5$

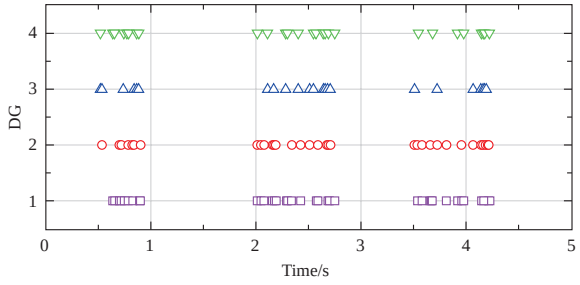

(b) $h = 1$, $\beta = 0.5$

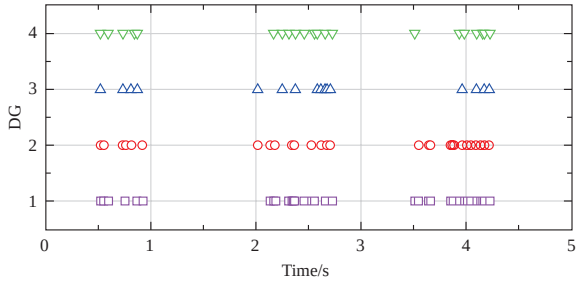

(c) $h = 0.7$, $\beta = 0.5$

Fig. 9 Triggering time instants at different clock rates

Table 2 Numbers of triggers under different clock rates

Clock rate	DG 1	DG 2	DG 3	DG 4
h=2	95	94	61	62
h=1	43	37	29	35
h=0,7	37	32	21	26

4 Conclusion

In this study, we established a distributed self-triggered active power-sharing control scheme by introducing a signum function and a linear clock. This design inherently excludes Zeno behavior in the controller. By improving the triggering condition, a substantial reduction in the computational and communication burdens on each DG controller was achieved without compromising control performance. The results verified that the proposed distributed self-triggered active power-sharing control successfully achieved a reduction of more than 99% in computation and communication requirements. This is particularly noteworthy for practical applications that address the coordination of renewable generation resources in new power systems.

Acknowledgments

This work was supported by Key Laboratory of Modern Power System Simulation and Control & Renewable Energy Technology (Northeast Electric Power University) Open Fund (MPSS2023-01), National Natural Science Foundation of China(No. 52477133), Hainan Provincial Natural Science Foundation of China (No. 524RC532), Research Startup Funding from Hainan Institute of Zhejiang University (No. 0210-6602-A12202) and Project of Sanya Yazhou Bay Science and Technology City (No. SKJC-2022-PTDX-009/010/011).

Declaration of Competing Interest

We declare that we have no conflict of interest.

References

[1] Yang S H, Lao K W, Chen Y L, et al. (2024) Resilient distributed control against false data injection attacks for demand response. IEEE Transactions on Power Systems, 39(2): 2837-2853

[2] Roy T K, Ghosh S K, Saha S (2023) Robust backstepping global integral terminal sliding mode controller to enhance dynamic stability of hybrid AC/DC microgrids. Protection and Control of Modern Power Systems, 8(1): 1-13

[3] Mortezapour V, Golshannavaz S, Pouresmaeil E, et al. (2022) A new hybrid control technique for operation of DC microgrid under islanded operating mode. Protection and Control of Modern Power Systems, 7(4): 1-11

[4] Jithin K, Haridev P P, Mayadevi N, et al. (2023) A review on challenges in DC microgrid planning and implementation. Journal of Modern Power Systems and Clean Energy, 11(5): 1375-1395

[5] Bidram A, Davoudi A (2012) Hierarchical structure of microgrids

control system. IEEE Transactions on Smart Grid, 3(4): 1963-1976
[6] Chen Y L, Huang X, Lao K W, et al. (2022) A zeno-free distributed self-triggered secondary control scheme for islanded microgrids. 2022 IEEE/IAS Industrial and Commercial Power System Asia (I&CPS Asia). Shanghai, China. IEEE,: 848-853
[7] Yang S H, Lao K W, Hui H X, et al. (2023) Real-time harmonic contribution evaluation considering multiple dynamic customers. CSEE Journal of Power and Energy Systems, PP(99): 1-13
[8] Shi Y, Cheng Y, Xie B, et al. (2023) An adaptive control strategy for microgrid secondary frequency based on parameter identification. Global Energy Interconnection, 6(5): 592-600
[9] Xu L, Guo Q L, Zeng H T, et al. (2024) Communication topology optimization for time-delay cyber-physical microgrids under distributed control. IEEE Transactions on Smart Grid, PP(99): 1
[10] Hui H X, Chen Y L, Yang S H, et al. (2022) Coordination control of distributed generators and load resources for frequency restoration in isolated urban microgrids. Applied Energy, 327: 120116
[11] Xin H H, Qu Z H, Seuss J, et al. (2011) A self-organizing strategy for power flow control of photovoltaic generators in a distribution network. IEEE Transactions on Power Systems, 26(3): 1462-1473
[12] Zhang G Y, Li C Y, Qi D L, et al. (2017) Distributed estimation and secondary control of autonomous microgrid. IEEE Transactions on Power Systems, 32(2): 989-998
[13] Bidram A, Davoudi A, Lewis F L, et al. (2013) Secondary control of microgrids based on distributed cooperative control of multi-agent systems. IET Generation, Transmission & Distribution, 7(8): 822-831
[14] Chen Y L, Qi D L, Dong H N, et al. (2021) A FDI attack-resilient distributed secondary control strategy for islanded microgrids. IEEE Transactions on Smart Grid, 12(3): 1929-1938
[15] Ansari S, Zhang J, Singh R E (2022) A review of stabilization methods for DCMG with CPL, the role of bandwidth limits and droop control. Protection and Control of Modern Power Systems, 7(1): 1-12
[16] Huo Z H, Xu C (2022) Event-triggered mechanism based robust fault-tolerant control for networked wind energy conversion system. Global Energy Interconnection, 5(1): 55-65
[17] Fan Y, Hu G Q, Egerstedt M (2017) Distributed reactive power sharing control for microgrids with event-triggered communication. IEEE Transactions on Control Systems Technology, 25(1): 118-128
[18] Chen Y L, Qi D L, Li Z M, et al. (2022) Distributed event-triggered control for frequency restoration in islanded microgrids with reduced trigger condition checking. CSEE Journal of Power and Energy Systems, PP(99): 1-10
[19] Wang Y, Nguyen T L, Xu Y, et al. (2019) Cyber-physical design and implementation of distributed event-triggered secondary control in islanded microgrids. IEEE Transactions on Industry Applications, 55(6): 5631-5642
[20] Abdolmaleki B, Shafiee Q, Seifi A R, et al. (2020) A zeno-free event-triggered secondary control for AC microgrids. IEEE Transactions on Smart Grid, 11(3): 1905-1916
[21] Choi J, Habibi S I, Bidram A (2022) Distributed finite-time event-triggered frequency and voltage control of AC microgrids. IEEE Transactions on Power Systems, 37(3): 1979-1994
[22] Zhao G L, Jin L Q, Wang Y F (2023) Distributed event-triggered secondary control for islanded microgrids with disturbances: A hybrid systems approach. IEEE Transactions on Power Systems, 38(2): 1420-1431
[23] Zhao G L, Hua C C (2021) A hybrid dynamic event-triggered approach to consensus of multiagent systems with external disturbances. IEEE Transactions on Automatic Control, 66(7): 3213-3220
[24] Yang H Q, Li T S, Long Y, et al. (2024) Event-triggered distributed secondary control with model-free predictive compensation in AC/DC networked microgrids under DoS attacks. IEEE Transactions on Cybernetics, 54(1): 298-307
[25] Chen Y L, Li C Y, Qi D L, et al. (2022) Distributed event-triggered secondary control for islanded microgrids with proper trigger condition checking period. IEEE Transactions on Smart Grid, 13(2): 837-848
[26] Nowzari C, Cortés J (2016) Distributed event-triggered coordination for average consensus on weight-balanced digraphs. Automatica, 68: 237-244
[27] Tahir M, Mazumder S K (2015) Self-triggered communication enabled control of distributed generation in microgrids. IEEE Transactions on Industrial Informatics, 11(2): 441-449
[28] Dimarogonas D V, Frazzoli E, Johansson K H (2012) Distributed event-triggered control for multi-agent systems. IEEE Transactions on Automatic Control, 57(5): 1291-1297
[29] Chen Y L, Lao K W, Qi D L, et al. (2023) Distributed self-triggered control for frequency restoration and active power sharing in islanded microgrids. IEEE Transactions on Industrial Informatics, 19(10): 10635-10646
[30] Gao H S, Xin H H, Huang L B, et al. (2022) Common-mode frequency in converter-integrated power systems: Definition, analysis, and quantitative evaluation. IEEE Transactions on Power Systems, 37(6): 4846-4860
[31] Bidram A, Lewis F L, Davoudi A (2014) Distributed control systems for small-scale power networks: Using multiagent cooperative control theory. IEEE Control Systems Magazine, 34(6): 56-77
[32] Wang Y, Tang J M, Si J D, et al. (2023) Power quality enhancement in islanded microgrids via closed-loop adaptive virtual impedance control. Protection and Control of Modern Power Systems, 8(1): 1-17
[33] Hong H H, Wang C, Xu G F, et al. (2023) Optimal control method of frequency in diesel generator based islanded microgrid. Electric Power Engineering Technology,42(6): 189-196
[34] Yue D W, Zhao W T, Yuan H H, et al. (2023) Reliability evaluation of islanded DC microgrid considering electric-hydrogen hybrid energy storage. Electric Power Engineering Technology, 42(3): 27-35
[35] Feng S, Yuan Z, Wang W Q, et al. (2023) Optimization and configuration of microgrid capacity based on LGPG-P2G in the context of carbon trading. Electric Power Engineering Technology,42(3): 157-167

Biographies

Yulin Chen received his BS in mathematics and applied mathematics and the MS degree in electrical engineering from Northeast Electric Power University, Jilin, China, in 2014 and 2017, respectively, and PhD degree in electrical engineering from Zhejiang University, Hangzhou, China, in 2021. He has authored or coauthored more than 30 journal papers published in IEEE Trans. Smart Grid, IEEE Trans. Indus. Informat., IEEE Trans. SMC. Systems, CSEE Journal of Power, and Energy Systems, etc.

His current research interests include distributed control of renewable energy and cyber-physical security with applications in smart grid.

Xing Huang received her BS degree in electrical engineering from China University of Mining and Technology, Xuzhou, China, 2022. She is working towards the PhD degree in electrical engineering with the School of Electrical Engineering, Zhejiang University, Hangzhou, China. Her research interests include distributed control strategy and cyber-physical security with applications in smart grid.

Guangxin Zhi received his PhD degree from North China Electric Power University, China. His research interests include ship and ocean engineering related design research, nuclear power transient monitoring and intelligent identification research, intelligent operation and maintenance of offshore wind power.

Shaohua Yang received his BS degree from Hefei University of Technology, Hefei, China, in 2017 and the MS degree from Fuzhou University, Fuzhou, China, in 2020, both in electrical engineering. He is currently working toward the PhD degree at University of Macau, Macao SAR, China. His research interests include cyber physical system, demand response, and power quality.

Hongxun Hui is an Assistant Professor with the State Key Laboratory of Internet of Things for Smart City, University of Macau. Previously, he received a BS degree in 2015 and PhD degree in 2020 both from the College of Electrical Engineering in Zhejiang University. From 2018 to 2019, he was a visiting scholar at the Advanced Research Institute in Virginia Tech and CURENT Center in University of Tennessee. His research interests are in the Internet of Things technologies for smart energy, optimization of integrated energy systems, control of flexible resources, and energy economics. He has authored/co-authored 1 international book, more than 50 SCI journal papers, and 16 issued patents. Three of the papers was selected as the ESI Highly Cited Papers (Top 1%).

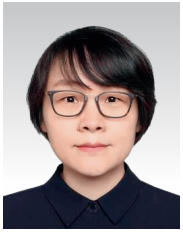

Donglian Qi received her PhD degree in control theory and control engineering from the School of Electrical Engineering, Zhejiang University, China, in 2002. She is currently a Full Professor and a PhD Advisor with Zhejiang University. Her research interests include intelligent information processing, chaos systems, and nonlinear theory and application.

Yunfeng Yan received her PhD degree in electrical engineering from Zhejiang University, Hangzhou, China, in 2019. She is currently an Associate Research Fellow with Zhejiang University. Her research interests include computer vision and machine learning systems, and distributed estimation and control of networked systems.

Fengkai Gao received the MS degree in Electrical Engineering in Northeast Electric Power University, Jilin, China, in 2018. At present, he works as an engineer at Northeast Electric Power University. His research interests include demand side management, demand response, and integrated energy system optimization.

(Editor Yanbo Wang)